CHEMISTRY
A EUROPEAN JOURNAL

DOI: 10.1002/chem.201100148

A Highly Selective, Cell-Permeable Fluorescent Nanoprobe for Ratiometric Detection and Imaging of Peroxynitrite in Living Cells

Jiangwei Tian, Huachao Chen, Linhai Zhuo, Yanxia Xie, Na Li, and Bo Tang*[a]

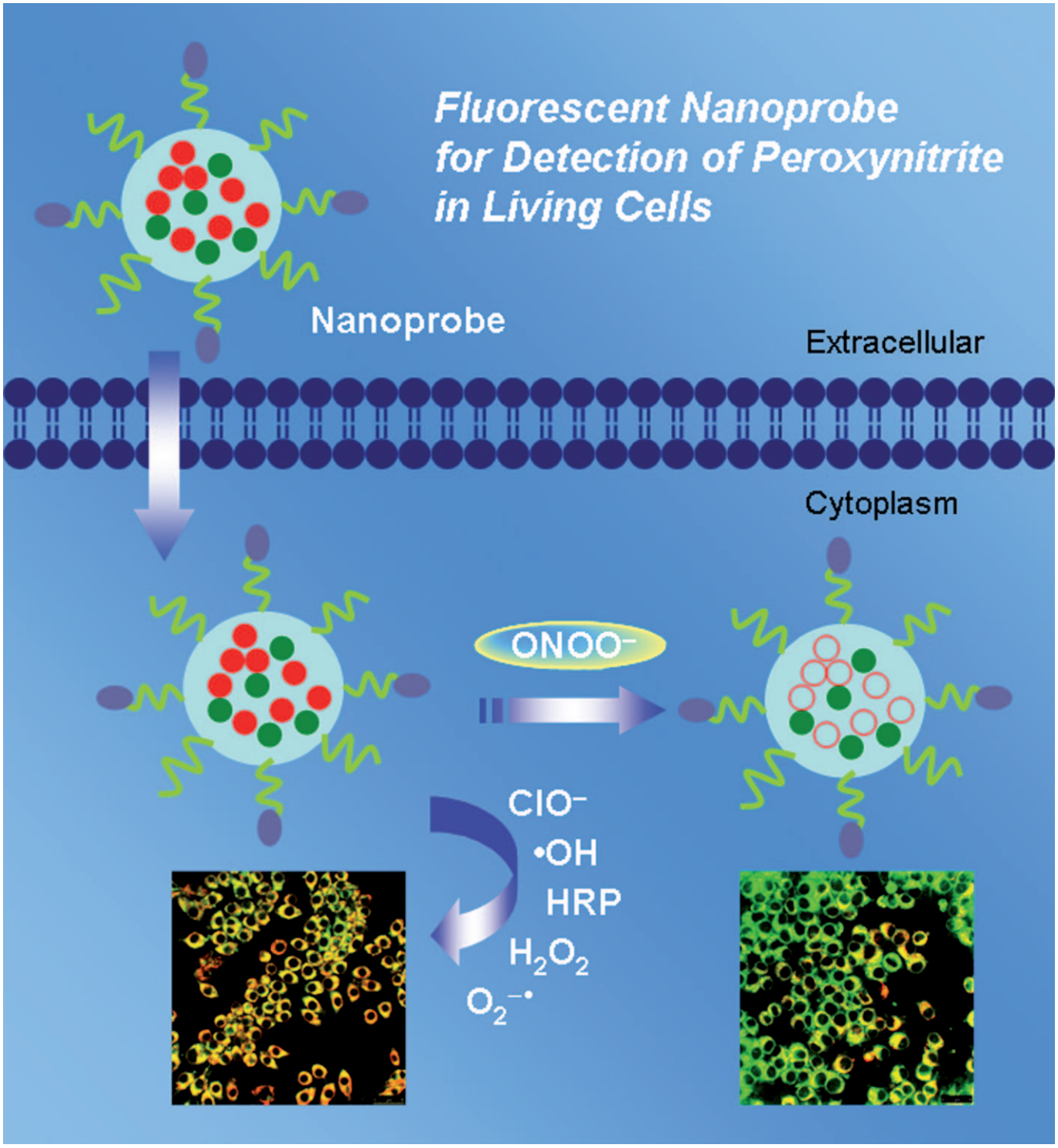

Abstract: Peroxynitrite ($ONOO^-$) is a highly reactive species implicated in the pathology of numerous diseases and there is currently great interest in developing fluorescent probes that can selectively detect $ONOO^-$ in living cells. Herein, a polymeric micelle-based and cell-penetrating peptide-coated fluorescent nanoprobe that incorporates $ONOO^-$ indicator dye and reference dye for the ratiometric detection and imaging of $ONOO^-$ has been developed. The nanoprobe effectively avoids the influences from enzymatic reaction and high-concentration $^{\bullet}OH$ and ClO^-. The improved $ONOO^-$ selectivity of the nanoprobe is achieved by a delicate complementarity of properties between the nanomatrix and the embedded molecular probe (BzSe-Cy). This nanoprobe also has other attractive properties, such as good water solubility, photostability, biocompatibility, and near-infrared excitation and emission. Fluorescence imaging experiments by confocal microscopy show that this nanoprobe is capable of visualizing $ONOO^-$ produced in living cells and it exhibits very low toxicity and good membrane permeability. We anticipate that this technique will be a potential tool for the precise pathological understanding and diagnosis of $ONOO^-$-related human diseases.

Keywords: bioimaging · fluorescent probes · nanoparticles · peptides · peroxynitrite

Introduction

Peroxynitrite ($ONOO^-$), formed in vivo from a diffusion-controlled reaction between nitric oxide ($^{\bullet}NO$) and superoxide ($O_2^{\bullet-}$),[1] is a highly reactive species implicated in the pathogenesis of numerous diseases, including inflammatory processes, ischemic reperfusion injury, multiple sclerosis, and neurodegenerative disorders.[2] This peroxide easily crosses biological membranes, and despite a relatively short half-life ($\approx$1 s) under physiological conditions, it can interact with various biological molecules, such as DNA, lipids, proteins, thiols, and metalloenzymes,[3] which may result in serious damage to living cells. To fully understand the biological effects of $ONOO^-$, a major focus of research is to exploit highly selective and sensitive methods to monitor the concentration changes of $ONOO^-$ in biosystems. Among these methods, spectrofluorimetry has become a powerful tool due to its high sensitivity and simplicity in data collection in imaging techniques.[4]

In recent years, many research efforts have focused on the development of fluorescence techniques for detecting $ONOO^-$. A variety of fluorescent probes, such as 3′-(*p*-aminophenyl)fluorescein (APF), dihydrorhodamine 123 (DHR-123) and dihydrodichlorofluorescein (DCFH) have been widely used to monitor $ONOO^-$ in various biosystems.[5] However, their fluorescence signals suffer from interferences by other reactive oxygen species (ROS), reactive nitrogen species (RNS) or unwanted enzymatic reactions. In particular, interferences from $^{\bullet}OH$ and ClO^- are severe obstacles in detecting $ONOO^-$ because of the similarity of $^{\bullet}OH$, ClO^-, and $ONOO^-$ with regard to their strong oxidation capacity.[6] To solve this problem, a few fluorescent probes, such as ketone oxidation-based HKGreen[7] and lanthanide-complex-based $[Eu^{3+}/Tb^{3+}(DTTA)]$[8], (DTTA = [4′-(2,4-dimethoxyphenyl)-2,2′:6′,2″-terpyridine-6,6″-diyl]bis(methylenenitrilo)tetrakis(acetic acid)) have been developed for the selective detection of $ONOO^-$. All of them are based on the specific reaction between a small-molecule probe and $ONOO^-$. However, utilizing a synergistic combination of nanomatrix and embedded $ONOO^-$-specific molecular probe to achieve higher selectivity for detecting $ONOO^-$ has not been reported to date.

Polymeric micelles, self-assembled nanoparticles from amphiphilic block copolymers, have many advantages in constructing multifunctional fluorescent nanoprobes. Micelle structures can incorporate different hydrophobic dyes in a single nanoparticle without complicated synthetic and separating procedures, so they offer a fascinating strategy for constructing ratiometric probes. The nanoparticles can be excited at the near-infrared (NIR) range by encapsulating NIR dyes, which leads to minimized photodamage and cell autofluorescence,[9] and also have stability in aqueous media and surface functionalization to act as biological probes.[10] Moreover, such nanoparticles exhibit higher brightness and better photostability than small-molecule dyes, owing to large numbers of chromophores per particle as well as the protective matrix.[11] As $ONOO^-$ is a highly permeable ROS,[12] another appealing feature of using a micelle structure is that the nanomatrix can enhance the selectivity of the embedded molecular probe toward $ONOO^-$ over other biologically relevant substances. Such induced selectivity can be achieved by a delicate complementarity of properties between the nanomatrix and the embedded molecular probe.[13] Based on the above, we attempted to develop a polymeric micelle-based nanoprobe that is highly specific for $ONOO^-$.

To further improve the cell-uptake efficiency of the nanoprobe for intracellular $ONOO^-$ imaging, a strong impe-

[a] J. Tian, H. Chen, L. Zhuo, Y. Xie, N. Li, Prof. B. Tang
College of Chemistry, Chemical Engineering and Materials Science
Key Laboratory of Molecular and Nano Probes
Engineering Research Center of Pesticide and Medicine Intermediate Clean Production, Ministry of Education
Shandong Provincial Key Laboratory of Clean Production of Fine Chemicals
Shandong Normal University, Jinan 250014 (P. R. China)
Fax: (+86) 531-8618-0017
E-mail: tangb@sdnu.edu.cn

Supporting information for this article is available on the WWW under http://dx.doi.org/10.1002/chem.201100148.

tus has been placed on the development of a nanoprobe with good cell permeability. Most methods that have been investigated to achieve the efficient intracellular delivery of nanoparticles (e.g., electroporation[14]) are limited to in vitro applications and often cause unwanted cellular effects, such as high cytotoxicity.[15] In recent years, use of cell-penetrating peptides (CPPs) conjugated to nanoparticles as an alternative strategy to facilitate their intracellular uptake has attracted broad interest and attention. CPPs which can enter cells in a nontoxic and highly efficient manner have been used successfully for the intracellular delivery of nanoparticles into the cell without disturbing the stability of the cell membrane and with low cytotoxic effects.[16] Thus, the use of these CPPs offers several advantages over conventional techniques because it is efficient for a range of cell types.

Herein, a hybrid polypeptide–polymer–organic dye nanoprobe for $ONOO^-$ has been designed and synthesized. The nanoarchitecture is composed of two key components: 1) a polymeric micelle that has a hydrophobic core made of poly(D,L-lactic acid) (PLA) and a hydrophilic shell consisting of polyethylene glycol (PEG) conjugated to CPPs; and 2) benzylselenide-tricarbocyanine (BzSe-Cy) as $ONOO^-$ indicator dye (Scheme 1) and isopropylrhodamine B (IRhB) as reference dye, which are simultaneously encapsulated in the hydrophobic core of the micelle for ratiometric $ONOO^-$ measurement. The details of this strategy are shown in Scheme 2. Because of its high diffusibility, $ONOO^-$ can rapidly diffuse into the core of the nanomatrix that blocks the entry of interferential bioanalytes and react with BzSe-Cy, thereby resulting in a dramatic fluorescence decrease, whereas the fluorescence of IRhB does not change, which leads to the selectively ratiometric detection of $ONOO^-$. Herein, the spectral characteristics of the nanoprobe were investigated under a simulated physiological environment, and the selectivity of free BzSe-Cy and the nanoprobe toward $ONOO^-$ were evaluated. Finally, the nanoprobe was applied to imaging of $ONOO^-$ in living macrophages (RAW 264.7), normal human liver cells (HL-7702), and human hepatoma cells (HepG2).

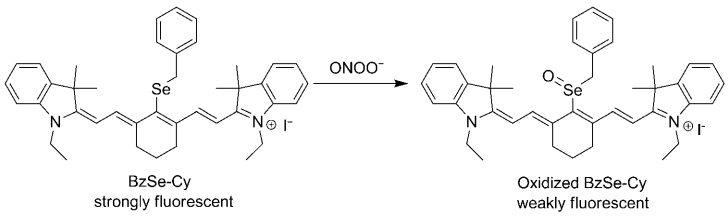

Scheme 1. Reaction of BzSe-Cy with $ONOO^-$.

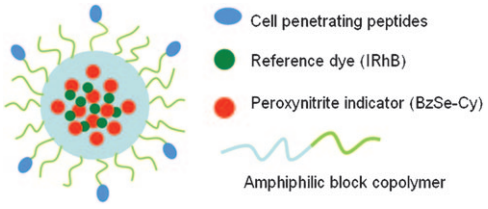

Scheme 2. Schematic illustration of the fabrication of a hybrid polypeptide–polymer–organic dye nanoprobe.

Results and Discussion

Design and synthesis of BzSe-Cy: We designed a hydrophobic NIR molecular probe (BzSe-Cy) that is sensitive to $ONOO^-$ (see Scheme 3 and Experimental Section). The relative fluorescence quantum yield of BzSe-Cy was 0.106, which was obtained by comparison with IR-786 in methanol ($\Phi = 0.159$), and the absorption coefficient was $28\,778\ M^{-1}cm^{-1}$ (see Supporting Information). The design strategy for BzSe-Cy is inspired by the specific reaction in which $ONOO^-$ oxidizes divalent selenium to quadrivalent selenium.[17] As indicated in Scheme 1, treatment of BzSe-Cy with $ONOO^-$ to generate the oxidized BzSe-Cy results in a significant fluorescence decrease. BzSe-Cy and its oxidized product have been verified by ESI-MS (Figure S1, Supporting Information) and ^{77}Se NMR spectroscopy (Figure S2).

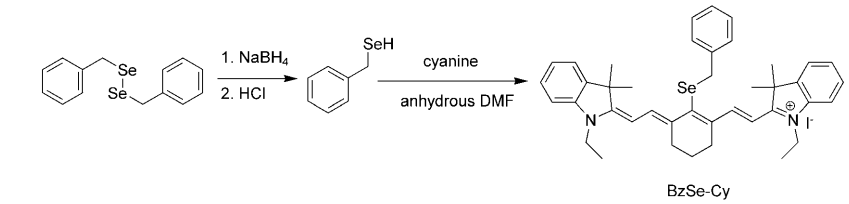

Scheme 3. Synthesis of BzSe-Cy; see the Experimental Section for details.

Synthesis and characterization of the nanoprobe: BzSe-Cy and IRhB were loaded into polymeric micelles by nanoprecipitation and self-assembly[18] at 2.9 and 0.05 wt%, respectively. In this study, amphiphilic block copolymers consisting of maleimide-terminated poly(ethylene glycol)-*block*-poly(D,L-lactide) (MAL-PEG-PLA) and methoxy-terminated poly(ethylene glycol)-*block*-poly(D,L-lactide) (MPEG-PLA) were used for micelle formation. Different amounts of MPEG-PLA were introduced to control the density of maleimide, which ultimately determined the density of CPPs on the micelle surface (0 and 10% of all PEG chains). CPPs were attached to the micelle surface through a covalent thiol–maleimide linkage.[19]

Transmission electron microscopy (TEM) and dynamic light scattering (DLS) were used for characterization of the

prepared nanohybrid. The TEM results indicate that the resulting particles in aqueous solution are well dispersed without aggregation, with mean hydrodynamic radius 54.7 nm as determined by DLS (Figure 1). The absorption spectrum

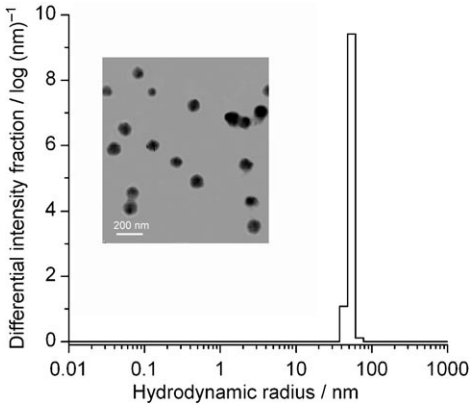

Figure 1. Dynamic light scattering curve of the nanoprobe. DLS samples were measured at a concentration of 0.25 mg mL^{-1} in 0.1 M phosphate-buffered saline (PBS, pH 7.4) at room temperature. Inset: Representative TEM image of the nanoprobe negatively stained with 2.0% phosphotungstic acid.

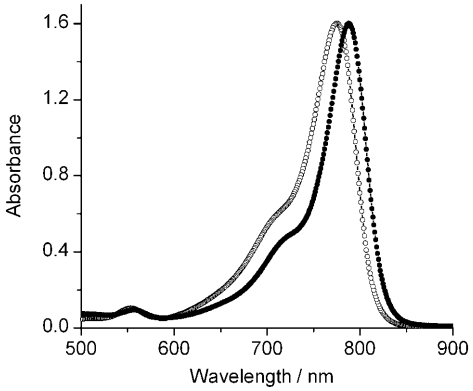

Figure 2. Absorption spectrum of the free dyes (○) in 0.1 M PBS solution (CH_3CN/H_2O, 2:8, pH 7.4) and the nanoprobes (●) in 0.1 M PBS solution (pH 7.4).

shows that the nanoprobe has two maximum absorption wavelengths, 555 nm for IRhB and 788 nm for BzSe-Cy (Figure 2). When the two dyes are finally encapsulated in the core of polymeric micelles, a slight red-shift of the absorption spectrum of IRhB and BzSe-Cy occurs, which is caused by the confinement of dye molecules in the micelle structures.[20] The nanoprobe can be excited at two different wavelengths to give different emission wavelengths (λ_{em} = 575, 810 nm). Confocal laser scanning microscopy (CLSM) studies were carried out to demonstrate that both IRhB and BzSe-Cy are in the same nanoparticle (Figure 3). When nanoparticles are excited at 532 nm, only IRhB can be excited and its associated green fluorescence is observed. Similarly, when the nanoparticles are excited at 635 nm, only BzSe-Cy can be excited and its associated red fluorescence is observed. When these two images are overlaid, they overlap completely, which demonstrates that both fluorophores are encapsulated in the same nanoparticle. Aqueous dispersions of the nanoprobe are clear and stable (Figure S3, Supporting Information), with negligible dye leakage (less than 1% at pH 7.4 in 80 h).

Photostability investigations: A highly desirable property of fluorescent probes is high resistance to photobleaching. We therefore investigated the photostability of free BzSe-Cy and the nanoprobe. Figure 4 shows changes in the relative fluorescence intensity (F/F_0) of free BzSe-Cy and the nanoprobe as a function of radiation time. The F/F_0 of free BzSe-Cy decreases by 50% within 60 min due to photon-induced chemical damage, whereas the F/F_0 of the nanoprobe does

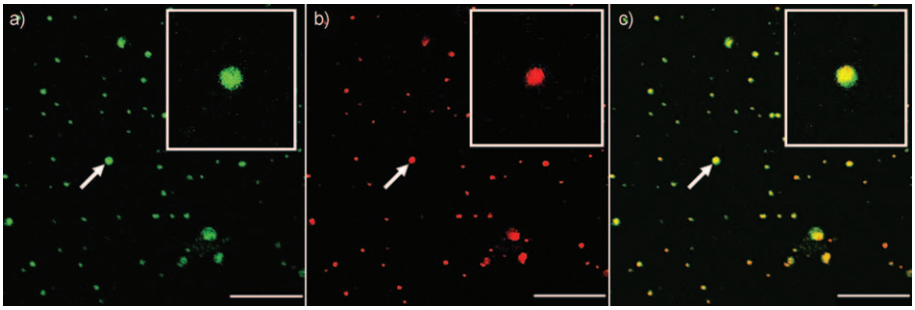

Figure 3. Confocal fluorescence images of the nanoprobe. Laser lines at a) 532 nm with emissions from 535 to 600 nm and b) 635 nm with emissions from 700 to 800 nm were used sequentially; c) overlay of panels (a) and (b). Scale bar: 25 μm.

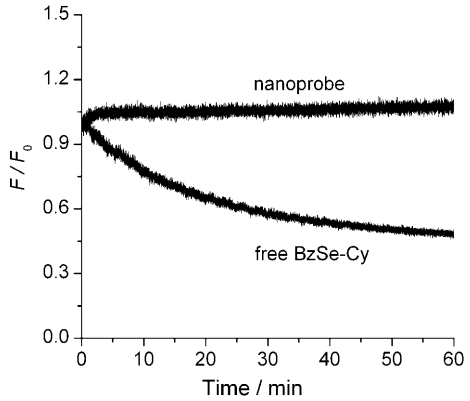

Figure 4. Relative fluorescence, $F/F_0 \rightarrow F_{t=t}/F_{t=0}$, of free BzSe-Cy (5 μM) in 0.1 M PBS solution (CH_3CN/H_2O, 2:8, pH 7.4) and the nanoprobe (0.25 mg mL^{-1}) in 0.1 M PBS, pH 7.4, after different radiation times with a 770 nm laser. The fluorescence emission intensity was measured at 800 nm.

not change over the same time period owing to the protection of the nanomatrix.[21] Similar results can be obtained for F/F_0 changes from free IRhB and the nanoprobe (Figure S4, Supporting Information). Therefore, the nanomatrix can effectively stabilize the fluorophore against oxidative degradation and makes a remarkably stable fluorescent nanoprobe.

Ratiometric detection of ONOO$^-$: Spectroscopic properties of the nanoprobe toward ONOO$^-$ were evaluated under simulated physiological conditions (0.1 M PBS, pH 7.4). Figure 5a shows the fluorescence emission spectra at 800–900 nm taken from the nanoprobe with ONOO$^-$. As expected, the fluorescence intensity is reduced successively with increasing ONOO$^-$ concentration. However, the fluorescence intensity at 575 nm is not influenced (Figure 5b). The fluorescence emission intensity ratio (F_{810}/F_{575}) varies from 2.49 in the absence of ONOO$^-$ to 0.16 after ONOO$^-$ treatment. Figure 5b shows the linear correlation ($R=0.9982$) between the F_{810}/F_{575} ratio and the relative amounts of added ONOO$^-$, within the concentration range of 0–5 μM. The detection limit was calculated to be 50 nM based on triplicate measurements of the relative standard. The nanoprobe therefore has the sensitivity to detect ONOO$^-$ in biosystems.

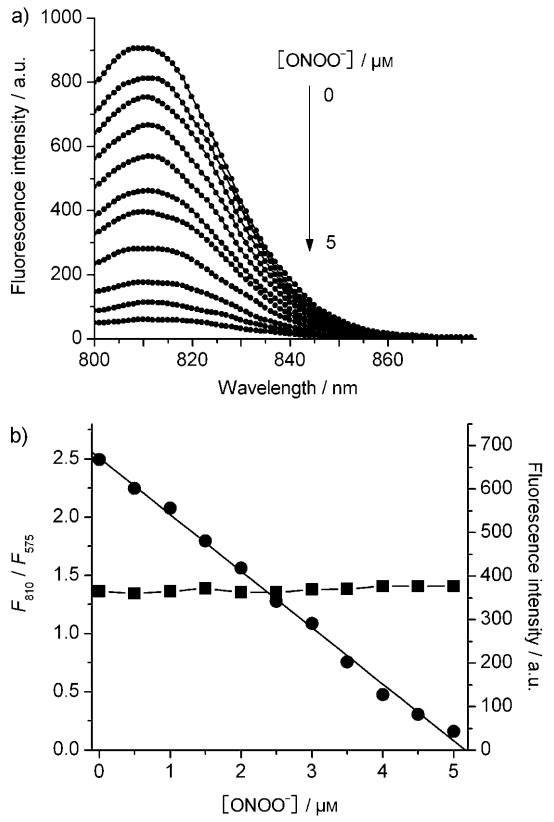

Figure 5. a) Fluorescence response of the nanoprobe (0.25 mg mL^{-1}) towards ONOO$^-$ with 788 nm excitation. Spectra shown are for ONOO$^-$ concentrations of 0, 0.5, 1.0, 1.5, 2.0, 2.5, 3.0, 3.5, 4.0, 4.5, and 5.0 μM. Spectra were acquired at room temperature in 0.1 M PBS, pH 7.4. b) Changes in fluorescence intensity at 575 nm with 555 nm excitation (squares, right *Y* scale) of the nanoprobe and the fluorescence intensity ratio F_{810}/F_{575} (circles, left *Y* scale) as a function of ONOO$^-$.

Kinetic assay: The fluorescence quenching kinetics of the ONOO$^-$–nanoprobe system was determined by real-time recording of the fluorescence intensity changes at $\lambda_{ex}/\lambda_{em}$ 788/810 nm after addition of ONOO$^-$. As shown in Figure 6, upon the addition of ONOO$^-$ at room temperature, a marked decrease in the intensity was obtained instantly up to 8 s and leveled off thereafter, which indicated the rapid response toward ONOO$^-$. Therefore, the nanoprobe has good reactivity for the detection of ONOO$^-$.

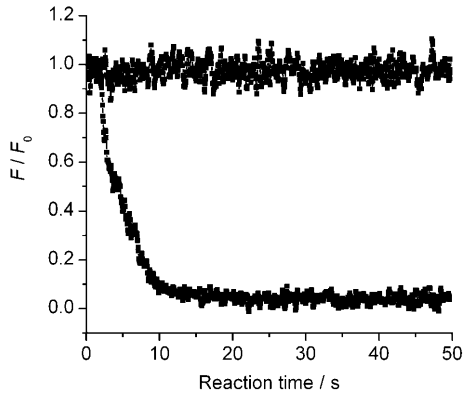

Figure 6. Fluorescence quenching kinetics curves of the nanoprobe (0.25 mg mL^{-1}) at 0 (top) and 5 μM (bottom) ONOO$^-$. Spectra were acquired at room temperature in 0.1 M PBS, pH 7.4 ($\lambda_{ex}=788$ nm, $\lambda_{em}=810$ nm).

Test for probe selectivity: The selectivity of the nanoprobe towards ONOO$^-$ was examined by monitoring the changes in F_{810}/F_{575} ratio upon exposure to various interfering agents, such as H_2O_2, $^1O_2$, and $^{\bullet}OH$. As shown in Figure 7, a 96% decrease in F_{810}/F_{575} ratio can be observed when the nano-

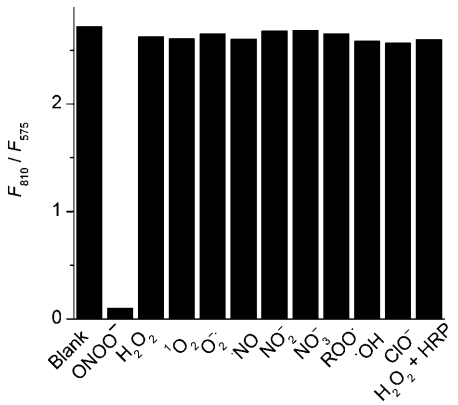

Figure 7. F_{810}/F_{575} ratio of the nanoprobe (0.25 mg mL^{-1}) in 0.1 M PBS solution (pH 7.4) with various biological analytes. Data were acquired at room temperature and the final concentrations of various analytes were 5 μM for ONOO$^-$, 500 μM for H_2O_2, $^1O_2$, $O_2^{\bullet-}$, $^{\bullet}NO$, NO_2^-, NO_3^-, and ROO$^{\bullet}$, 450 μM for $^{\bullet}OH$, 250 μM for ClO^-, and 10 μM for HRP.

probe is reacted with 5 μM $ONOO^-$, whereas the reactions of the nanoprobe with other biologically relevant substances, including H_2O_2, $^1O_2$, $O_2^{-\bullet}$, $^\bullet NO$, NO_2^-, NO_3^-, $ROO^\bullet$ (500 μM), H_2O_2/horseradish peroxidase (HRP; 500/10 μM), $^\bullet OH$ (450 μM), and ClO^- (250 μM), could not induce the change of F_{810}/F_{575} ratio (change $<5\%$). We also investigated the fluorescence responses of free BzSe-Cy to various analytes. As shown in Figure S6a and S6b in the Supporting Information, BzSe-Cy is specific for $ONOO^-$ when other analytes are in a certain concentration range (50 μM for $^\bullet OH$ and ClO^-, 500 μM for others). The selectivity to $ONOO^-$ is due to the specific reaction in which $ONOO^-$ oxidizes divalent selenium to quadrivalent selenium, and to the relatively high oxidation potential of free BzSe-Cy (0.622 V, see Supporting Information), which meant that BzSe-Cy was not oxidized easily by ROS.[22] However, as shown in Figure S6b in the Supporting Information, it suffers interferences from enzymatic reaction (H_2O_2/HRP) and highly oxidizing analytes with high concentrations (450 μM for $^\bullet OH$ and 250 μM for ClO^-). In contrast, when BzSe-Cy was encapsulated in the nanoparticle, it showed excellent selectivity even in the high-concentration ROS solution (Figure 7). The enhanced specificity of the nanoprobe is attributed to the nanomatrix that blocks the interferences from other biological analytes. Significantly, $ONOO^-$ has high diffusibility (the permeability coefficient is 8.0×10^{-4} cm s^{-1} which is $\approx$400 times greater than that of $O_2^{-\bullet}$)[23] and could rapidly diffuse into the hydrophobic core of the nanomatrix and react with BzSe-Cy. By contrast, other ROS such as $O_2^{-\bullet}$ and ClO^- with relatively low diffusibility find it hard to permeate the nanomatrix. $^\bullet OH$ has the shortest lifetime (nanoseconds or shorter) among all the ROS, and does not have enough time to penetrate into the nanomatrix. The nanomatrix resistance to HRP interference is due to the large size of the HRP, which is too large to penetrate into the nanomatrix. The same size exclusion may also eliminate potential confounding interactions from other enzymes or macromolecules. It is quite evident that the nanomatrix is beneficial to the enhanced specificity of the nanoprobe for $ONOO^-$.

Fluorescence imaging of intracellular $ONOO^-$ in RAW 264.7 macrophages: We next sought to apply such a nanoprobe to ratiometric fluorescence imaging of $ONOO^-$ in living cells. We investigated the potential of the nanoprobe to image $ONOO^-$, generated by activated macrophages, in a 3-morpholinosydnonimine (SIN-1) model.[24] The ratiometric fluorescence images were monitored in RAW 264.7 macrophages treated with different oxidants, namely the $ONOO^-$ donor SIN-1, the $^\bullet NO$ donor *S*-nitroso-*N*-acetyl-DL-penicillamine (SNAP), and the $O_2^{-\bullet}$ donor xanthine/xanthine oxidase. The macrophages were incubated with nanoprobes (0.03 mg mL^{-1}) for 60 min and then washed three times with PBS buffer. The ratio images were constructed from 700 to 800 nm (red) and from 535 to 600 nm (green) fluorescence collection windows. As expected, treatment of nanoprobe-loaded cells with 10 μM SIN-1 triggers a dramatic decrease in the red-to-green emission ratio (Figure 8b), but not with either SNAP (Figure 8c) or xanthine/xanthine oxidase (Figure 8d). The mean fluorescence intensity ratio from the living cells was also quantified with Image-Pro software (Figure 8e), and demonstrated that the SIN-1-treated cells had an approximately 45% decrease in fluorescence intensity ratio, which is much more than that of other groups (5 and 8%, respectively). Thus, we conclude that this nanoprobe can be used for the selective imaging of $ONOO^-$ produced in cultured cells. Moreover, bright-field measurements and Hoechst-33258 staining confirmed that the cells are viable throughout the imaging studies (Figure 8b and Figure S7, Supporting Information). Taken together, these results suggest that the nanoprobe has the potential for studying biological processes involving $ONOO^-$ within living cells.

Fluorescence imaging in HL-7702 and HepG2 cells: Considering that the majority of cells in the human body are nonphagocytic, confocal fluorescence imaging experiments were carried out in other biological models to further verify the feasibility of the nanoprobe. Extensive studies demonstrate that tumor occurrence is related to ROS.[25] Therefore, we selected HL-7702 and HepG2 cells to investigate whether this nanoprobe can detect $ONOO^-$ in nonphagocytic cells (Figure 9). Images reveal that there are fluorescence distinctions between normal cells and tumor cells. These results indicate that the probe can be used for detecting $ONOO^-$ in a variety of cells, which foreshadows broad application prospects of the nanoprobe in biological systems.

Test for cell permeability of the nanoprobe: To enhance cell permeability of the nanoprobe for intracellular imaging, CPPs were attached to the micelle surface to facilitate the internalization of the nanoprobe. Flow cytometry and CLSM were used to evaluate the effect of CPPs on nanoparticle uptake. Figure 10 shows the flow cytometry histogram after 0 and 10% CPP micelles were incubated with macrophages for 60 min. An obvious increase in cell uptake is observed with 10% CPP micelles over 0% CPP micelles, thus demonstrating that the CPP-encoded nanoprobe is more cell-permeable for intracellular imaging. To further study the cell permeability of the nanoprobe (10% CPP micelles), the interactions of the cells with nanoprobe at 4 and 37°C was investigated. Nanoprobe internalization was studied at 4°C to mitigate energy-dependent endocytic pathways. As shown in Figure S9 in the Supporting Information, the intracellular fluorescence is still apparent at 4°C, which confirms that the nanoprobe has good cell permeability and is suitable for fluorescence imaging in biological samples.

MTT assay: To evaluate the cytotoxicity of the nanoprobe, we performed MTT (3-(4,5-dimethylthiazol-2-yl)-2,5-diphenyltetrazolium bromide) assay in macrophages with nanoprobe concentrations of 0.005, 0.01, 0.015, 0.02, 0.03, 0.05, 0.10, and 0.25 mg mL^{-1}. The results show that the nanoprobe exhibits almost no cytotoxicity or side effects for the incubation (Figure S10, Supporting Information).

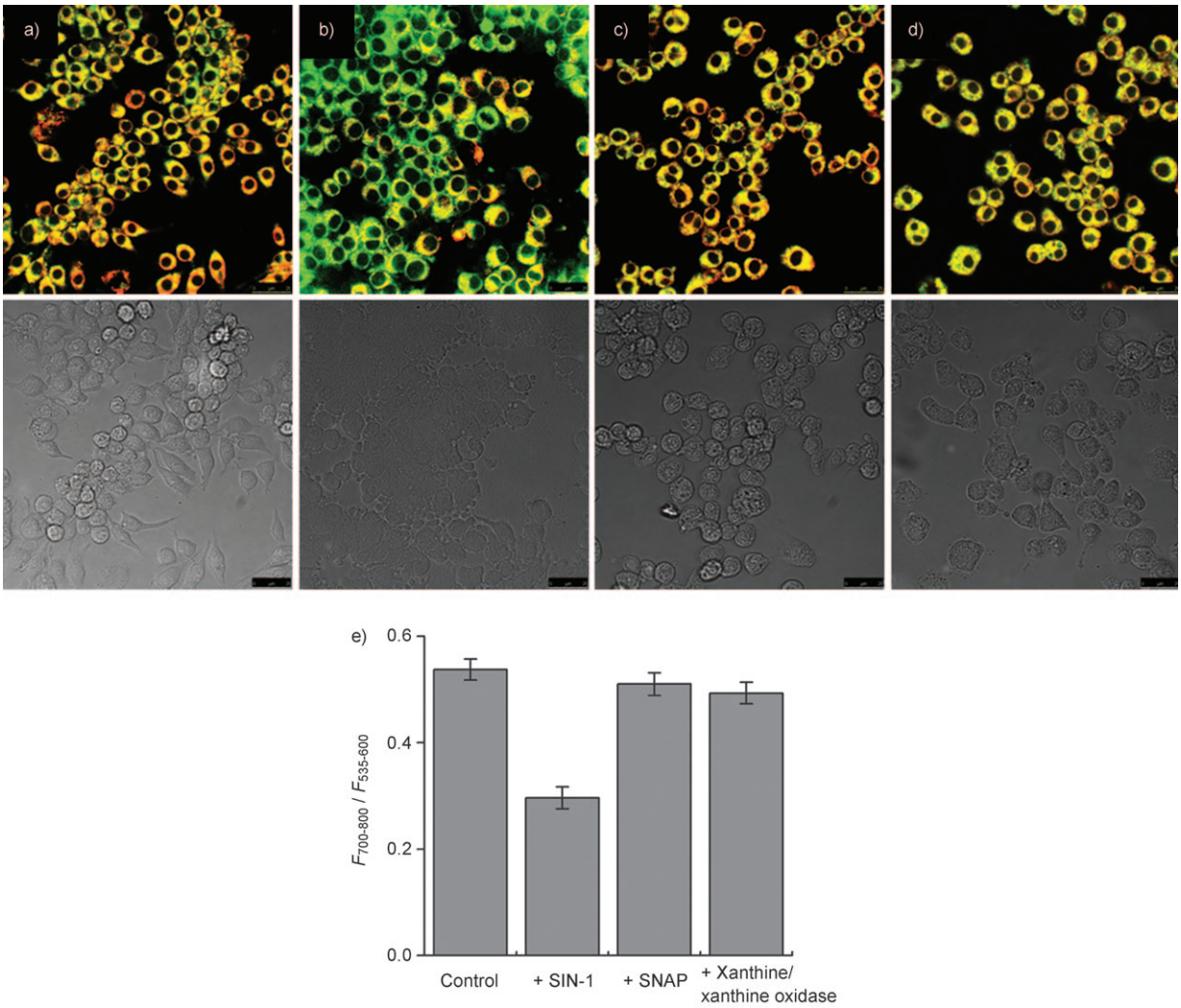

Figure 8. a)–d) Confocal, ratiometric fluorescence images of RAW 264.7 macrophage cells. Top: Images displayed in pseudocolor represent the ratio of emission intensities collected in optical windows of 700–800 (red) and 535–600 nm (green). Bottom: Bright-field images. The macrophages were incubated with 0.03 mg mL^{-1} nanoprobe for 60 min at 37 °C and then subjected to different treatments. a) Control; b) 10 μM SIN-1; c) 10 μM SNAP; d) 100 μM xanthine and 0.1 IU xanthine oxidase. Scale bar: 25 μm. e) Bar graph representing the integrated intensity from 700 to 800 nm over the integrated fluorescence intensity from 535 to 600 nm. Values are the mean ratio generated from the intensity from five randomly selected fields. Error bars represent standard error measurement (s.e.m.).

Conclusion

We have developed a hybrid polypeptide–polymer–organic dye nanoprobe that is highly sensitive and selective for the ratiometric detection of $ONOO^-$. The molecular probe BzSe-Cy is specific for $ONOO^-$, and the selectivity can be further improved by encapsulating BzSe-Cy in the nanoparticle for using as a nanoprobe. Additional experiments demonstrate that the new probe has the unique advantages of good water solubility, photostability, biocompatibility, and NIR excitation and emission. Furthermore, ratiometric fluorescence imaging establishes the good cell permeability and capability of visualizing intracellular $ONOO^-$ of this nanoprobe. We anticipate that this nanoprobe will be a potential tool for the precise pathological understanding and diagnosis of $ONOO^-$-related human diseases.

Experimental Section

Materials: Unless stated otherwise, solvents were dried by distillation. All reagents were of commercial quality and used without further purification. Isopropylrhodamine B (IRhB) and 2-[4-chloro-7-(1-ethyl-3,3-dimethylindolin-2-ylidene)]-3,5-(propane-1,3-diyl)-1,3,5-(heptatrien-1-yl)-1-ethyl-3,3-dimethyl-3*H*-indolium (Cy.7.Cl) were synthesized in our laboratory. Methoxy-polyethylene glycol (MPEG, $M_n = 2000$ Da), stannous(II) octoate ($Sn(Oct)_2$), 3-morpholinosydnonimine (SIN-1), 3-(4,5-dimethylthiazol-2-yl)-2,5-diphenyltetrazolium bromide (MTT), 2,2′-azobis(2-amidinopropane) dihydrochloride (AAPH), xanthine (X; 1 mM) in 10 mM NaOH solution, xanthine oxidase (XO; 5 U mL^{-1}), *S*-nitroso-*N*-acetyl-DL-penicillamine (SNAP), sodium nitroferricyanide(III) dihydrate (SNP), and horseradish peroxidase (HRP) were purchased from Sigma Chemical Company. D,L-Lactide (99% pure) and dibenzyl diselenide (95+%) were purchased from Alfa Aesar Chemical Company. Maleimide–polyethylene glycol (maleimide-PEG-OH, $M_n = 2900$ Da) was purchased from Shanghai Yare Biotech, Inc. TAT CPPs (Gly-Arg-Lys-Lys-Arg-Arg-Gln-Arg-Arg-Arg-Pro-Pro-Gln-Cys) were purchased from Chinese Peptide

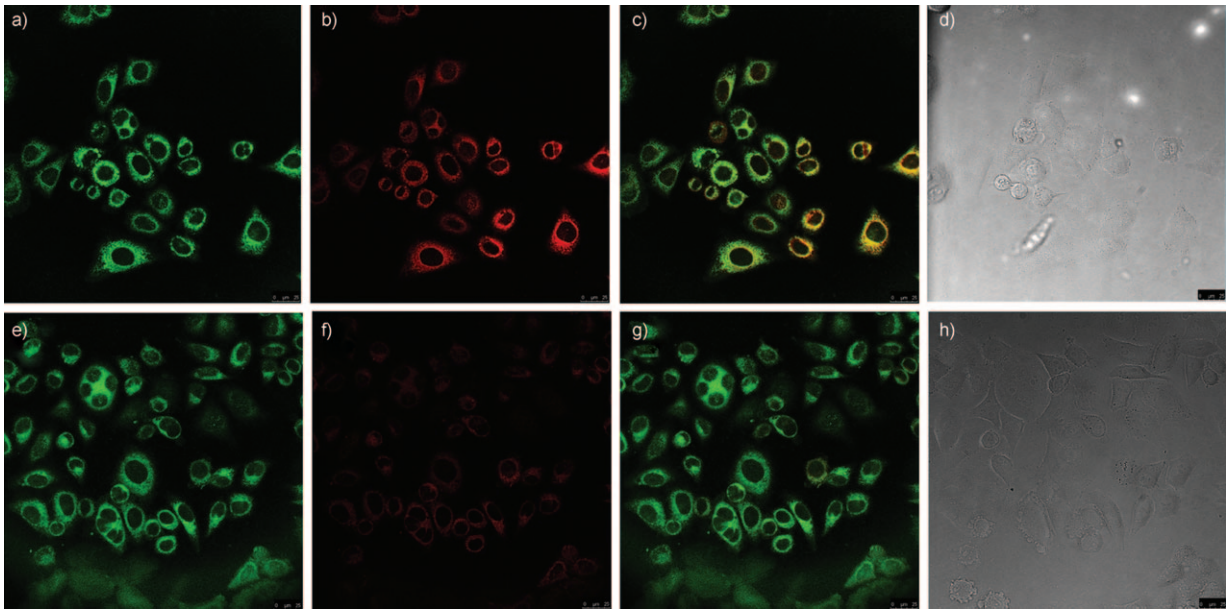

Figure 9. Confocal fluorescence images of living HL-7702 (a–d) and HepG2 (e–h) cells. HL-7702 and HepG2 cells were separately incubated in 0.03 mg mL^{-1} nanoprobe for 60 min and then were rinsed three times with PBS. The green channel (a, e) represents the fluorescence collected at 535–600 nm, and the red channel (b, f) represents the fluorescence collected at 700–800 nm. Images c) and g) represent merged images of red and green channels. Images d) and h) represent bright-field images of cells in panels a)–c) and e)–g), respectively. Scale bar: 25 μm.

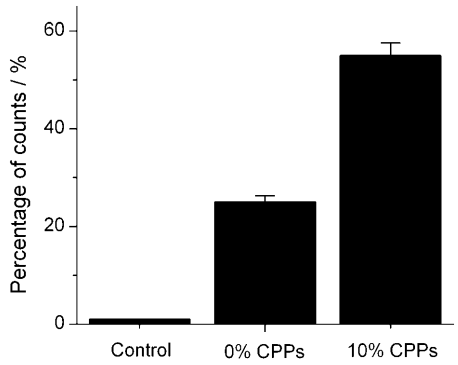

Figure 10. Flow cytometry histogram of nanoprobe uptake in RAW 264.7 macrophages as a function of encoding CPPs. Error bars represent s.e.m.

Company. Sartorius ultrapure water (18.2 MΩ cm) was used throughout the analytical experiments. RAW 264.7 macrophage cells, human liver (HL-7702) cells, and human hepatoma (HepG2) cells were purchased from the Committee on Type Culture Collection of the Chinese Academy of Sciences.

Apparatus: Particle size was determined by the DLS method with a DynaProTitan instrument (Wyatt Technology Corp., USA). Samples were diluted and the hydrodynamic radius of a micelle was determined. TEM was carried out on a JEM-100CX Π electron microscope. Fluorometric traces were obtained with a Cary Eclipse fluorescence spectrophotometer (Varian, Inc., USA) equipped with a 1.0 cm quartz cell at the slits of 5/10 nm. Absorption spectra were measured on a PharmaSpec UV-1700 UV–visible spectrophotometer (Shimadzu). The release tests of IRhB and BzSe-Cy in vitro were performed with an Agilent 1100 Series HPLC system. All pH measurements were performed with a pH-3c digital pH meter (Shanghai Lei Ci Device Works, Shanghai, China) with a combined glass–calomel electrode. ^{1}H and ^{13}C NMR spectra were obtained on Bruker Avance 600 MHz and ^{77}Se NMR Bruker 300 MHz spectrometers. The fluorescence images of cells were taken by using an LTE confocal laser scanning microscope (Germany Leica Co., Ltd.). Absorbance was measured in a Triturus microplate reader in the MTT assay. Flow cytometry analysis was carried out on a CytomicsTM FC 500 flow cytometer.

Synthesis of BzSe-Cy: According to the synthesis of a series of NIR cyanine dyes proposed by Peng,[26] with some modification, we synthesized the new probe BzSe-Cy (Scheme 3). Solid $NaBH_4$, (0.26 g, 6.9 mmol) was added over a 15 min period to a suspension of dibenzyl diselenide (1.021 g, 3 mmol) in absolute ethanol (60 mL) cooled to 0 °C under a stream of nitrogen. After completion of the addition, the mixture was allowed to warm to room temperature and stirred for 30 min to give a clear solution. This reaction was quenched with 5% HCl (20 mL) and extracted with ether/pentane (1:1, 3×10 mL). The organic phase was dried over anhydrous sodium sulfate and the solvent was evaporated. The benzylselenol was obtained as a colorless foul-smelling oil. DMF (15 mL) was added to benzylselenol, and then cyanine (0.196 g) was added to the solution. The mixture was stirred at 43 °C under Ar for 48 h. Finally, the mixture was purified by silica gel chromatography with elution by ethyl acetate/methanol (4:1 v/v) to give BzSe-Cy as a green solid (55% yield). ^{1}H and ^{13}C NMR spectra were recorded on a Bruker Avance 600 MHz spectrometer and ^{77}Se NMR spectra were recorded on a Bruker 300 MHz spectrometer. ^{1}H NMR (600 MHz, [D$_6$]acetone, 25 °C): δ = 8.80 (d, J = 12.6 Hz, 2H), 7.60 (d, J = 7.2 Hz, 2H), 7.40–7.47 (m, 4H), 7.29 (t, J = 7.2 Hz, 2H), 7.25 (d, J = 7.8 Hz, 2H), 7.16–7.23 (m, 3H), 6.37 (d, J = 14.4 Hz, 2H), 4.31 (q, J = 6.6 Hz, 4H), 4.12 (s, 2H), 2.71 (t, J = 6.6 Hz, 4H), 1.86 (m, 2H), 1.71 (s, 12H), 1.42 ppm (t, J = 6.0 Hz, 6H); ^{13}C NMR (600 MHz, [D$_6$]acetone, 25 °C): δ = 206.07, 172.95, 158.50, 150.14, 143.03, 142.15, 139.95, 134.98, 129.57, 129.56, 129.31, 127.92, 125.87, 123.34, 111.62, 101.75, 50.06, 39.92, 34.81, 27.91, 27.18, 21.87, 12.54 ppm; ^{77}Se NMR (300 MHz, CD$_3$CN, 25 °C): δ = 265 ppm; MS: m/z: calcd 647.9 $[M]^+$, found 647.5; elemental analysis (%) calcd: C 63.6, H 6.1, N 3.6; found C 63.7, H 6.2, N 3.7.

Synthesis of MPEG-PLA and MAL-PEG-PLA: The MPEG-PLA and MAL-PEG-PLA diblock copolymers were synthesized by ring-opening polymerization as described previously.[27] In brief, predetermined amounts of MPEG or maleimide-PEG and D,L-lactide were placed in a dried round-bottomed bottle connected with a vacuum joint. In both cases, an appropriate amount of stannous octoate was added as a solution in dried toluene. The reactants were dried under reduced pressure at

70 °C for 1 h, and then the reaction proceeded under vacuum at 160 °C for 4 h. The cooled product was dissolved in dichloromethane, and recovered by precipitation into an excess of mixed solvent comprising ethyl ether and petroleum ether. The precipitate was redissolved in acetone and precipitated into excess water, with the purified copolymers dried in a vacuum oven at 40 °C for 24 h and then stored in a desiccator under vacuum. The two copolymers were analyzed by ^{1}H NMR spectroscopy at room temperature. The degree of polymerization of the PLA was calculated by comparing the integral intensity of the characteristic resonance of the PLA at 5.2 ppm (−C(=O)−C**H**(−CH_3−)) and PEG resonance at 3.64 ppm (−OC**H$_2$**C**H$_2$**−) in the ^{1}H NMR spectrum (Figure S11, Supporting Information). The amount of maleimide proton was calculated by comparing the integral intensity of the characteristic resonance at 6.70 ppm and PEG resonance at 3.64 ppm (−OC**H$_2$**C**H$_2$**−). MAL-PEG-PLA (M_n = 28.6 kD) was synthesized and used in this study.

Synthesis of the hybrid polypeptide–polymer–organic dye nanoprobe: The CPPs-encoding nanoprobe loaded with two dyes was prepared by nanoprecipitation and self-assembly.[18] Briefly, MPEG-PLA (9 mg mL^{-1}), MAL-PEG-PLA (1 mg mL^{-1}), BzSe-Cy (0.5 mM), and IRhB (0.01 mM) were dissolved in acetonitrile and together mixed dropwise into water, giving a final polymer concentration of 1.0 mg mL^{-1}. The solution was vortexed vigorously for 3 min followed by self-assembly under gentle stirring for 2 h at room temperature, and the remaining organic solvent was removed in a rotary evaporator at reduced pressure. The nanoparticles were centrifuged at 14000 × *g* for 15 min and washed with deionized water. The TAT peptide was conjugated to the maleimide on the PEG of the micelles through a thioether linkage. The polymeric micelles in PBS, with maleimide groups on the outside of the shell, were mixed with a small molar excess of TAT peptide solution at pH 7.2 under a nitrogen atmosphere. The mixture was stirred overnight in the dark at room temperature. The TAT-conjugated micelles were then separated from unreacted TAT by using a PD10 column in PBS. Finally, the resulting solution was filtered with a 220 nm pore size cellulose acetate filter and stored at 4 °C.

Acknowledgements

This work was supported by the National Basic Research Program of China (973 Program, 2007CB936000), National Natural Science Funds for Distinguished Young Scholars (No. 20725518), National Key Natural Science Foundation of China (No. 21035003), Natural Science Foundation of Shandong Province in China (No. ZR2010BZ001), and Science and Technology Development Programs of Shandong Province of China (No. 2008GG30003012).

[1] a) G. Ferrer-Sueta, R. Radi, *ACS Chem. Biol.* **2009**, *4*, 161–177; b) S. Goldstein, J. Lind, G. Merényi, *Chem. Rev.* **2005**, *105*, 2457–2470; c) C. Szabó, H. Ischiropoulos, R. Radi, *Nat. Rev. Drug Discovery* **2007**, *6*, 662–680.

[2] a) P. Pacher, J. S. Beckman, L. Liaudet, *Physiol. Rev.* **2007**, *87*, 315–424; b) J. S. Beckman, M. Carson, C. D. Smith, W. H. Koppenol, *Nature* **1993**, *364*, 584–585; c) H. Ischiropoulos, J. S. Beckman, *J. Clin. Invest.* **2003**, *111*, 163–169.

[3] a) C. Szabó, H. Oshima, *Nitric Oxide* **1997**, *1*, 373–385; b) J. T. Groves, *Curr. Opin. Chem. Biol.* **1999**, *3*, 226–235; c) R. P. Patel, J. McAndrews, H. Sellak, R. C. White, H. Jo, B. A. Freeman, V. M. Darley-Usmar, *Biochim. Biophys. Acta Bioenerg.* **1999**, *1411*, 385–400.

[4] a) A. Gomes, E. Fernandes, J. L. Lima, *J. Biochem. Biophys. Methods* **2005**, *65*, 45–80; b) B. Halliwell, M. B. Whiteman, *J. Pharmacol.* **2004**, *142*, 231–255.

[5] a) K. Setsukinai, Y. Urano, K. Kakinuma, H. J. Majima, T. Nagano, *J. Biol. Chem.* **2003**, *278*, 3170–3175; b) N. W. Kooy, J. A. Royall, H. Ischiropoulos, J. S. Beckman, *Free Radical Biol. Med.* **1994**, *16*, 149–156; c) H. Possel, H. Noack, W. Augustin, G. Keilhoff, G. Wolf, *FEBS Lett.* **1997**, *416*, 175–178.

[6] a) P. Li, T. Xie, X. Duan, F. Yu, X. Wang, B. Tang, *Chem. Eur. J.* **2009**, *15*, 1834–1840; b) C. A. Cohn, C. E. Pedigo, S. N. Hylton, S. R. Simon, M. A. Schoonen, *Geochem. Trans.* **2009**, *10*, 8.

[7] D. Yang, H. L. Wang, Z. N. Sun, N. W. Chung, J. G. Shen, *J. Am. Chem. Soc.* **2006**, *128*, 6004–6005.

[8] C. Song, Z. Ye, G. Wang, J. Yuan, Y. Guan, *Chem. Eur. J.* **2010**, *16*, 6464–6472.

[9] D. Wu, A. B. Descalzo, F. Weik, F. Emmerling, Z. Shen, X. Z. You, K. Rurack, *Angew. Chem.* **2008**, *120*, 199; *Angew. Chem. Int. Ed.* **2008**, *47*, 193–197.

[10] a) W. C. Wu, C. Y. Chen, Y. Tian, S. H. Jang, Y. Hong, Y. Liu, R. Hu, B. Z. Tang, Y. T. Lee, C. T. Chen, W. C. Chen, A. K. Y. Jen, *Adv. Funct. Mater.* **2010**, *20*, 1413–1423; b) K. Li, J. Pan, S. S. Feng, A. W. Wu, K. Y. Pu, Y. Liu, B. Liu, *Adv. Funct. Mater.* **2009**, *19*, 3535–3542.

[11] a) H. Ow, D. R. Larson, M. Srivastava, B. A. Baird, W. W. Webb, U. Wiesner, *Nano Lett.* **2005**, *5*, 113–117; b) Z. F. Li, E. Ruckenstein, *Nano Lett.* **2004**, *4*, 1463–1467.

[12] a) R. Radi, *Chem. Res. Toxicol.* **1998**, *11*, 720–721; b) A. Denicola, J. M. Souza, R. Radi, *Proc. Natl. Acad. Sci. USA* **1998**, *95*, 3566–3577.

[13] G. Kim, Y. E. K. Lee, H. Xu, M. A. Philbert, R. Kopelman, *Anal. Chem.* **2010**, *82*, 2165–2169.

[14] F. Q. Chen, D. Gerion, *Nano Lett.* **2004**, *4*, 1827–1832.

[15] J. L. Cohen, A. Almutairi, J. A. Cohen, M. Bernstein, S. L. Brody, D. P. Schuster, J. M. J. Fréchet, *Bioconjugate Chem.* **2008**, *19*, 876–881.

[16] a) V. A. Sethuraman, Y. H. Bae, *J. Controlled Release* **2007**, *118*, 216–224; b) B. Gupta, T. S. Levchenko, V. P. Torchilin, *Adv. Drug Delivery Rev.* **2005**, *57*, 637–651.

[17] a) S. Padmaja, G. L. Squadrito, J. N. Lemercier, R. Cueto, W. A. Pryor, *Free Radical Biol. Med.* **1996**, *21*, 317–322; b) C. W. Nogueira, G. Zeni, J. B. T. Rocha, *Chem. Rev.* **2004**, *104*, 6255–6285.

[18] a) O. C. Farokhzad, J. Cheng, B. A. Teply, I. Sherifi, S. Jon, P. W. Kantoff, J. P. Richie, R. Langer, *Proc. Natl. Acad. Sci. USA* **2006**, *103*, 6315–6320; b) H. Chen, S. Kim, L. Li, S. Wang, K. Park, J. X. Cheng, *Proc. Natl. Acad. Sci. USA* **2008**, *105*, 6596–6601.

[19] N. Nasongkla, E. Bey, J. Ren, H. Ai, C. Khemtong, J. S. Guthi, S. F. Chin, A. D. Sherry, D. A. Boothman, J. Gao, *Nano Lett.* **2006**, *6*, 2427–2430.

[20] G. Rainò, T. Stöferle, C. Park, H. C. Kim, I. J. Chin, R. D. Miller, R. F. Mahrt, *Adv. Mater.* **2010**, *22*, 3681–3684.

[21] M. Akbulut, P. Ginart, M. E. Gindy, C. Theriault, K. H. Chin, W. Soboyejo, R. K. Prud′homme, *Adv. Funct. Mater.* **2009**, *19*, 718–725.

[22] D. Oushiki, H. Kojima, T. Terai, M. Arita, K. Hanaoka, Y. Urano, T. Nagano, *J. Am. Chem. Soc.* **2010**, *132*, 2795–2801.

[23] S. S. Marla, J. Lee, J. T. Groves, *Proc. Natl. Acad. Sci. USA* **1997**, *94*, 14243–14248.

[24] C. Q. Li, L. J. Trudel, G. N. Wogan, *Chem. Res. Toxicol.* **2002**, *15*, 527–535.

[25] J. M. McCord, *Science* **1974**, *185*, 529–531.

[26] F. Song, X. Peng, E. Lu, Y. Wang, W. Zhou, J. Fan, *Tetrahedron Lett.* **2005**, *46*, 4817–4820.

[27] Y. Zhang, Q. Z. Zhang, L. S. Zha, W. L. Yang, C. C. Wang, X. G. Jiang, S. K. Fu, *Colloid Polym. Sci.* **2004**, *282*, 1323–1328.

Received: January 15, 2011
Published online: May 17, 2011

